Journal of Marine Research, 56, 1259–1284, 1998

Comparative diagenesis at three sites on the Canadian continental margin

by Bernard P. Boudreau[1], Alfonso Mucci[2], Bjorn Sundby[3], George W. Luther[4] and Norman Silverberg[5]

ABSTRACT

Diagenesis of carbon, oxygen, nitrogen, and manganese at three sites on the Canadian continental margin is quantitatively compared and contrasted using results from a computer code (CANDI) published by Boudreau (1996a). The data at Station 3 (Cabot Strait) are well explained by the steady state output from CANDI, assuming a porewater balance created by diffusion and reaction only, whereas the data from Stations 4 (Emerald Basin-Scotia Shelf) and 5 (Scotia Slope) are not consistent, in one way or another, with this simple model. The deviations between model and data at Station 4 are best explained by nonsteady-state diagenesis. Model fits to the Station 5 ΣCO_2 observations are improved dramatically by adding some irrigation at this site, but the ΣNH_3 distribution appears to be subject to an additional anomalous transport to the O_2 zone and subsequent oxidation to NO_3^-. The mechanism for this latter phenomena is unknown and in need of future research.

In addition, the O_2 and ΣCO_2 profiles at all sites require the existence of at least two reactive organic matter types; furthermore, the initial amounts of these OM types at each station is strongly dependent on the intensity of particle bioturbation. Ammonia is preferentially regenerated at Station 3 at a high ratio of about 25 N to 106 C. The net kinetics of the deeper removal of Mn^{2+} appear to be fractional-order with respect to the concentration of this species, suggesting multiple removal processes. Finally, an oxidant balance, assuming steady state, indicates a considerable difference in the use of oxidants at each station even though the O_2 fluxes are similar.

1. Introduction

Much of early diagenesis is driven by the regeneration of organic carbon (Berner, 1980; Canfield, 1993). Because of the shallow water column, proximity to land and nutrient sources, continental margin sediments receive a greater proportion of the net primary productivity than equivalent sediments in the deep sea. This fact is reflected in the much higher concentrations of organic carbon in shelf and slope sediments. Moreover, Berner (1982) showed that the total burial rate of organic carbon in marginal sediments is

1. Department of Oceanography, Dalhousie University, Halifax, Nova Scotia, B3H 4J1, Canada.
2. Department of Earth and Planetary Sciences, McGill University, Montréal, QC, H3A 2A7, Canada.
3. INRS-Oceanologie, Université du Québec, Rimouski, QC, G5L 3A1, Canada.
4. College of Marine Studies, University of Delaware, Lewes, Delaware, 19958, U.S.A.
5. CICIMAR-IPN, Playa el Conchalito S/N, AP 592, Lapaz, Baja California Sur 23000, Mexico.

presently about six times that in pelagic sediments, due to greater sedimentation rates that overwhelm the effect of the relatively small surface area. As a result, diagenetic processes in continental margin sediments play a far greater role globally in the removal and regeneration of organic carbon and nutrients than similar processes in abyssal sediments. No study of the fluxes and fate of carbon in the oceans can be considered complete or accurate without considering benthic carbon cycling in continental margin sediments.

Our understanding of the processes that dominate organic matter diagenesis and their rates in marginal sediments remains surprisingly slim. A major contributing factor to this situation is the heterogeneity of this environment with respect to sediment type, accumulation rates, degrees of biological and physical disturbance, and geochemical composition and inputs. At the same time, sampling of porewaters and fluxes has proven to be difficult in some sediments; i.e., sands and gravels. Even for muds, which are amenable to standard sampling technologies, the number of geochemically documented sites outside of shallow coastal areas is relatively small compared to deep-sea locations.

Although a better accounting of diagenesis in coarser sediments will require more methodological innovation, we are, nevertheless, in a position to improve our quantitative knowledge of diagenesis in muddy sediments of the continental margin. To this aim, the Canadian JGOFS program (CJGOFS) has conducted a comprehensive porewater sampling program at three stations on the Eastern Canadian Continental Margin—described later in this paper. Separate subsets of the resulting analyses have been reported and discussed in individual papers on mixing, iron and manganese chemistries, oxygen fluxes, calcium-carbonate dissolution/precipitation, etc. (i.e., Anschutz *et al.,* 1998; Luther *et al.,* 1998; Mucci *et al.,* 1999; Mulsow *et al.,* 1998; Silverberg *et al.,* 1999); nevertheless, an integrated evaluation of these data and their full implication to diagenesis in marginal environments has yet to appear.

Once a diagenetic data set has been obtained, a quantitative description of the processes that have produced these observations is not possible without some form of modeling (Berner, 1980). Modeling of continental margin porewaters is particularly difficult because of the extensive couplings between different species, the variety of oxidants utilized, and the nonlinear kinetics that characterize organic matter decay and by-product oxidation reactions. In response, various advanced computer codes have been developed recently to deal with such complications; e.g., Boudreau (1996a), Soetaert *et al.* (1996), Van Cappellen and Wang (1995), and Wang and Van Cappellen (1996). Applications of these codes are still rare and more need to appear in the literature in order to allow potential users to fully evaluate code utility, strengths and weaknesses. The CJGOFS data set presents an opportunity to illustrate the use of one of these codes, i.e. CANDI (*C*arbon *a*nd *N*utrient *Di*agenesis), as presented in Boudreau (1996a).

Before jumping into the presentation of the application and its results, a short discussion of the philosophy behind this modeling effort is in order so as to avoid false expectations and misunderstandings. When a model does not reproduce a *reliable* set of data, this situation does not constitute a failure of modeling per se. A *properly-formulated and*

constructed model is nothing more than a canonical form of our collective understanding of a chosen geochemical system. A mismatch questions our understanding, not the modeling exercise. In fact, lack of agreement between a correctly formulated and solved model and data is normally more informative than coherence. A negative outcome unquestionably indicates a problem in the content of the model and, consequently, in our logic or comprehension. On the other hand, the reason for model-data consistency can never be established without a doubt; that is to say, the model may be a correct representation of the phenomena being examined or the agreement may be the result of excessive flexibility of the model solution. For example, the exponential function is the solution to a number of steady-state models cast as differential equations; e.g., burial-decay equation, diffusion-decay equation, diffusion-advection equation, etc. (see Boudreau, 1997). Exponentials are renown for their mathematical elasticity, such that they can be made to fit almost any data set. Goodness of model fit to a data set can hardly be the basis for proclaiming the correctness of a model in this situation.

2. Data

Detailed descriptions of the station locations, the data and the sampling and analytical techniques are available in the papers by Mulsow *et al.* (1998), Anschutz *et al.* (1998), Luther *et al.* (1998), Mucci *et al.* (1999), and Silverberg *et al.* (1999). Discussion of faunal species, abundances, bioturbational activity can be found in Grehan *et al.* (1994). Only a brief overview is provided here.

a. Sites & sampling

Sediment cores were collected from three stations located on the Eastern Canadian Continental Margin during a June 1994 cruise of the CSS *Hudson*. A map showing the geographic location of the sites is provided in Mulsow *et al.* (1998) and Luther *et al.* (1998) and, in order to save journal space, is not repeated here. Station 3 (47°30′N, 60°05′W) is at a depth of 525 m in the Laurentian Trough (roughly Station 12 of Silverberg *et al.,* 1986), Station 4 (43°50′N, 62°49′W) is at 230 m in the center of a small basin on the continental shelf (see Buckley, 1991 and Grant *et al.,* 1991 for detailed geological descriptions), and Station 5 (42°53′N, 61°45′W) is located on the continental slope at a depth of 780 m. Samples for porewater and solids analyses were collected with a 0.12 m^2 box corer, while those intended for micro-electrode and flux measurements were obtained with a Bowers & Connelly multicorer.

b. Data

Porewater modeling with CANDI will focus on the depth distributions of O_2, NO_3^-, ΣCO_2, ΣNH_3, and Mn^{2+}. These particular data were chosen because they constitute the minimal data set needed by CANDI for internal consistency in estimating parameter values. The O_2 concentration was measured with two types of micro-electrodes, polaro-

graphic Clark-type electrode and a solid-state voltammetric electrode (Silverberg *et al.,* 1999; Luther *et al.,* 1997) at *in situ* temperature on board ship after retrieval of the multicorer. The NO_3^-, ΣCO_2 and ΣNH_3 were obtained on squeezed porewater samples, as described in Anschutz *et al.* (1998) and Mucci *et al.* (1999). The O_2 and NO_3^- data are supplemented by independent measurements of their fluxes at the sediment-water interface, determined on board ship following time-series incubations (Luther *et al.,* 1998). The dissolved manganese data were obtained with a solid-state voltammetric microelectrode (Luther *et al.,* 1997). The data are illustrated in Figures 1 through 8 later in this paper. In addition to these porewater measurements, porosity profiles and excess ^{210}Pb were obtained in order to determine bioturbation rates, as presented in Mulsow *et al.* (1998).

3. The model—CANDI

Details of the construction and workings of CANDI are provided in Boudreau (1996a). Like the chemical analyses, these details are not repeated here. Briefly, CANDI has the capability to model the effects of transport processes (molecular diffusion of solutes, biodiffusion of solids, burial, compaction, and irrigation of solutes) and various reactions (organic matter decay, by-product oxidation of Mn^{2+}, NH_4^+, H_2S, etc., FeS and FeS_2 precipitation and oxidation, $CaCO_3$ dissolution, and solid-solid reactions, e.g. FeS + MnO_2, etc.) on the distributions of organic matter, nutrients, oxidants, reduced by-products, acid-base speciation and pH in an aqueous sediments.

For each solute species, the conservation (diagenetic) equations are of the form:

$$\frac{\partial C}{\partial t} = \frac{1}{\varphi}\frac{\partial}{\partial x}\left(\varphi D'_C \frac{\partial C}{\partial x} - \varphi u C\right) + \eta(x)[C_o - C] - \Sigma R \tag{1}$$

where C is the concentration of the solute (mM of porewater), t is time (years), x is depth (cm), φ is porosity, D'_C is the tortuosity-corrected molecular diffusivity (cm^2 yr^{-1}), u is the porewater advection velocity (cm yr^{-1}), $\eta(x)$ is the rate constant for irrigation as a function of depth (yr^{-1}), C_o is the concentration at the sediment-water interface (mM), and ΣR is the sum of reactions (mM yr^{-1}).

Specific forms of ΣR assumed in CANDI are listed in Boudreau (1996a) and are largely those found in Wang and Van Cappellen (1996). The primary modification has been to include a few new reactions, i.e. (Aller 1990; Luther *et al.,* 1997):

$$5Mn^{2+} + 2NO_3^- + 4H_2O \rightarrow 5MnO_2 + N_2 + 8H^+ \tag{2}$$

and

$$NO_3^- + H_2S + H_2O \rightarrow SO_4^{2-} + NH_4^+ \tag{3}$$

Reactions between nitrate and FeS and FeS_2 probably also occur, but these are not considered in this paper. Information and data with regard to the kinetics of reactions (2) and (3) are nonexistent; consequently, following the lead of Van Cappellen and Wang

(1995), plausible kinetic expressions are postulated to be

$$R_{MnNO_3} = -k_{MnNO_3}(Mn^{2+})(NO_3^-) \tag{4}$$

$$R_{H_2SNO_3} = -k_{H_2SNO_3}(H_2S)(NO_3^-) \tag{5}$$

for reactions (2) and (3), respectively.

In addition, the data presented below will show that Mn^{2+} is also removed from below the oxic zone by solid-phase interactions. A variety of processes can produce this phenomenon; i.e., co-precipitation with $CaCO_3$ (e.g., Pedersen and Price, 1982; Thomson *et al.,* 1986; Aller and Rude, 1988; Mucci, 1988), adsorption onto $CaCO_3$ or FeS surfaces (Arakaki and Morse, 1993), and/or the formation of a distinct $MnCO_3$ phase (e.g., Boyle, 1983; Middelburg *et al.,* 1987). Because the specific process(es) acting at our stations remains unidentified, the kinetics of suboxic Mn^{2+} removal are initially modeled as first order in the concentration of that species, i.e.

$$R_{Mn-loss} = -k_{Mn-loss}(Mn^{2+}). \tag{6}$$

First-order kinetics for these reactions are at best gross over-simplifications; nevertheless, in some circumstances, irreversible adsorption can be approximated as first order (Boudart and Djéga-Mariadassou, 1984), and (co)-precipitation may appear to be first order if the rate of formation of the mineral is relatively constant over the zone of Mn^{2+} removal. The values of all rate constants are reported later.

Each component of the solids obeys an equation similar to Eq. (1):

$$\frac{\partial B}{\partial t} = \frac{1}{\varphi_s}\frac{\partial}{\partial x}\left(\varphi_s D_B(x)\frac{\partial B}{\partial x} - \varphi_s w B\right) - \Sigma R_B \tag{7}$$

where B is the concentration of a solid species (mmoles per dm^3 of solids), φ_s is solids volume fraction ($1 - \varphi$), D_B is the bioturbational diffusivity ($cm^2\ yr^{-1}$), w is the solids advection velocity ($cm\ yr^{-1}$), and ΣR_B is the sum of reactions affecting the solid being modeled (mmoles per dm^3 of solids yr^{-1}). The values of the various parameters in these equations are given below. These equations are solved numerically by the method of lines (see Boudreau, 1996a, 1997).

4. Parameter values

General diagenetic codes, such as CANDI, contain a host of free parameters; i.e., diffusion, irrigation, and bioturbation coefficients, rate and Monod constants, whose values must be specified in order to produce a model outcome (prediction). Some are best reserved for fitting the data; e.g., organic matter stoichiometric coefficients and decomposition rate constants, because they are of fundamental importance (see next section), but others are either reasonably well known *a priori;* e.g., diffusion coefficients, or play more minor roles

and are best fixed prior to model runs. The values for the latter type parameters are discussed below.

Free-solution diffusion coefficients in pure water for all solutes in the model are calculated with the formulas in Boudreau (1997, Chapter 4, Section 4.2.3). Temperature, pressure and salinity corrections were obtained using the formulas from Li and Gregory (1974) and Kukulka *et al.* (1987). To correct for tortuosity, the porosity profiles are fit to an exponential formula (Mulsow *et al.,* 1998) and the empirical equation advanced by Boudreau (1996b) is utilized; i.e., $\theta^2 = 1 - \ln(\varphi^2)$, where θ is the tortuosity. This $\theta - \varphi$ relationship is valid for the entire natural range of these variables. All calculations are made automatically in CANDI.

Bioturbation is assumed to be dominantly diffusional at our three stations, which is consistent with faunal abundances, distributions and species types, but minor head-down deposit feeding probably occurs at Stations 3 and 5 (Grehan *et al.,* 1994); nevertheless, ^{210}Pb distributions are adequately described by a diffusional model (Mulsow *et al.,* 1998) and that practice is continued here. Using excess ^{210}Pb profiles and assuming constant porosity, Mulsow *et al.* (1998) derive D_B values of 0.19 and 0.37 cm^2 yr^{-1} for Stations 4 and 5, respectively, in the summer of 1994. The lower D_B value at Station 4 is consistent with the lower abundances and bioturbational capacity of the fauna at that station (Grehan *et al.,* 1994). Station 3 was characterized by values of 12.1 cm^2 yr^{-1} in the 0–5 cm zone and 0.68 cm^2 yr^{-1} between 5–16 cm. This latter depth-dependence was approximated using a Gaussian function as in Christensen (1982). Calculated D_B values for all these stations at other sampling times (i.e., May 1993 and December 1993) exhibit a fair amount of variability (see Tables 3, 4 and 5 in Mulsow *et al.,* 1998) which is probably related to pronounced local heterogeneities (Smith and Schaffer, 1984), because seasonal variability usually cannot be resolved with ^{210}Pb profiles. In calculating D_B values, all the penetration of excess ^{210}Pb was attributed to mixing; this is certainly not true, as burial must also contribute. The burial velocity was set to a nominal value of 0.01 cm yr^{-1} at all stations (see Mucci *et al.,* 1998), while noting that larger values have modest effect on the porewater profiles modeled here. Furthermore, the irrigation rate constant was set initially to zero in the model results given below, but nonzero values were later explored in fitting the data at Station 5.

The plethora of reactions included in CANDI, as well as their kinetics, can be found in Boudreau (1996a). The values for preset rate constants for the present study are given in Table 1; obvious rate constants not found in this table will be discussed in the next section. The exact numerical value of most of the rate constants for the by-product oxidation reactions are not known, but they are thought to be large and any value above 10^3 mM^{-1} yr^{-1} produces essentially the same result within the errors in the data. Also, a zero value for a particular constant does not represent its true value or that this reaction does not occur at the CJGOFS sites, simply that the reaction was not considered.

Organic matter oxidation is assumed to have a Monod-type dependence on the concentrations of the various available oxidants (Boudreau and Westrich, 1984; Boudreau,

Table 1. Values for preset rate constants in CANDI used in modeling the CJGOFS Stations.

Reaction	Equation number†	Station 3	Station 4	Station 5	Units
Mn^{2+} oxidation with NO_3^-	(2)	1.0×10^4	1.0×10^5	1.0×10^5	$mM^{-1}\ yr^{-1}$
ΣH_2S oxidation with NO_3^-	(3)	1.0×10^4	1.0×10^5	1.0×10^5	$mM^{-1}\ yr^{-1}$
ΣH_2S oxidation with O_2	B (10)	1.0×10^7	1.0×10^6	1.0×10^6	$mM^{-1}\ yr^{-1}$
Mn^{2+} oxidation with O_2	B (9)	1.0×10^5	1.0×10^5	1.0×10^5	$mM^{-1}\ yr^{-1}$
Fe^{2+} oxidation with O_2	B (8)	1.0×10^5	1.0×10^5	1.0×10^5	$mM^{-1}\ yr^{-1}$
ΣNH_4 oxidation with O_2	B (11)	1.0×10^7	1.0×10^7	1.0×10^7	$mM^{-1}\ yr^{-1}$
FeS oxidation with O_2	B (19)	1.0×10^3	0	0	$mM^{-1}\ yr^{-1}$
FeS oxidation with MnO_2	B (18)	0	0	0	$mM^{-1}\ yr^{-1}$
FeS oxidation with Fe^{3+}	B (17)	0	0	0	$mM^{-1}\ yr^{-1}$
ΣH_2S oxidation with Fe^{3+}	B (16)	10	10	10	$mM^{-1}\ yr^{-1}$
FeS formation	B (7)	3	300	300	$mM^{-1}\ yr^{-1}$
FeS_2 formation	B (20)	1.0×10^{-3}	1.0×10^{-3}	1.0×10^{-3}	yr^{-1}
Fe^{2+} oxidation with MnO_2	B (14)	10	10	10	$mM^{-1}\ yr^{-1}$
ΣH_2S oxidation with MnO_2	B (15)	1	10	10	$mM^{-1}\ yr^{-1}$
CH_4 oxidation with O_2	B (12)	1.0×10^5	1.0×10^5	1.0×10^5	$mM^{-1}\ yr^{-1}$
CH_4 oxidation with $SO_4^=$	B (13)	1.0×10^5	1.0×10^5	1.0×10^5	$mM^{-1}\ yr^{-1}$

†Equations numbers preceded by a B indicate equations in Boudreau (1996a). Many values taken from Van Cappellen and Wang (1995).

1996a, 1997; Van Cappellen *et al.,* 1993; and Van Cappellen and Gaillard, 1996). The Monod saturation constants for O_2, NO_3^- and $SO_4^=$ are 0.08, 0.015 and 1.0 mM, respectively, at all stations.

Bottom waters ($x = 0$) were not sampled and analyzed separately for each station. A uniform water composition at the sediment surface of 0.2 mM O_2, 0.032 mM NO_3^-, 0.011 mM ΣNH_4, 0.0 mM Mn^{2+}, 0.0 mM Fe^{2+} and 0.0 mM CH_4 was assumed for each station. The ΣCO_2 was 2.303 mM at Stations 3 and 4 and 2.25 mM at Station 5. The ammonia concentration is assumed, not measured in June 1994; it is undoubtedly too high, but that fact is of no consequence. The dissolved sulfate was calculated from the bottom water chlorinities, Cl, using the equation $SO_4^= = Cl \cdot 0.00145753$.

CANDI was run to steady state at each station with either 1000 or 2000 points on the modeled depth interval. The interval varied from 35 cm at Stations 4 and 5 to as much as 150 cm at Station 3.

5. Results and discussion

In conducting our analysis, perfect fits to the data sets are not possible, in part because couplings in the reaction terms of the diagenetic equations cause interdependence between model predictions for different species, and because the data do not originate from the same cores, the effects of lateral heterogeneities add variability. An optimal (eye-ball) fit for one species may cause a less than acceptable fit to another; consequently, the results displayed

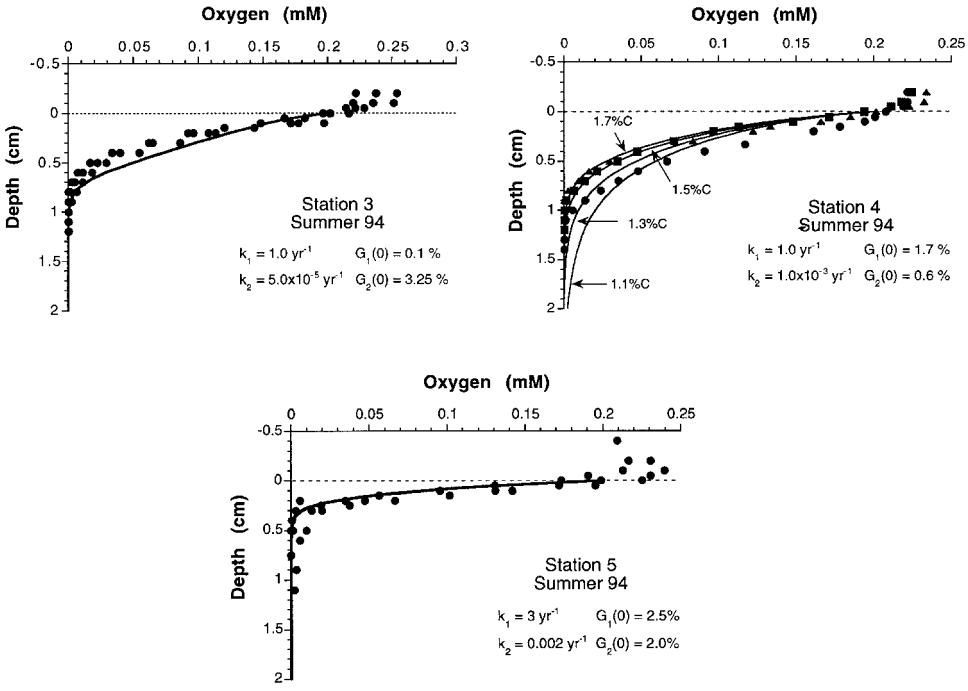

Figure 1. Oxygen data collected with microelectrodes at Station 3, 4 and 5. The solid lines are eye-balled best fits with the program CANDI (Boudreau, 1996a). Each diagram also contains the value of the decay constants for each of the two reactive organic matter types and their respective concentrations at the sediment-water interface.

here are compromise solutions, and the underlying need for these compromises will be discussed, when appropriate.

a. Oxygen

The microelectrode-measured O_2 profiles are displayed in Figure 1, and the solid lines are fits from CANDI. Least-squares fitting of the Bouldin (1968) model can produce statistically superior approximations to this data than that provided by CANDI (Luther *et al.,* 1997; Silverberg *et al.,* 1999); nevertheless, the CANDI-based fits are better than acceptable, and the reader must remember that CANDI is constrained to fit more than one species simultaneously. In addition, the interfacial O_2 flux generated from the CANDI fit (see Table 2) for Station 3 is statistically identical to the chamber-measured value of -4.14 ± 0.95 mmole m^{-2} d^{-1}, whereas the model-calculated values are within a factor of two to three of the measured values at the other two sites; i.e., -4.9 ± 0.08 mmole m^{-2} d^{-1} at Station 4 and -4.4 ± 0.85 mmole m^{-2} d^{-1} at Station 5 (see Luther *et al.,* 1997).

CANDI requires the existence of two types of reactive organic matter in order to simulate the observed O_2 and ΣCO_2 profiles (see below). The Station 4 plot (Fig. 1, upper right-hand diagram) illustrates typical model sensitivity to the surficial ($x = 0$) fraction of

Table 2. Summary of parameters and other quantities derived with CANDI from the CJGOFS data assuming steady state.

Parameter†	Station 3	Station 4	Station 5	Units
$G_1(0)$	0.1	1.7	2.5	% of solids
$G_2(0)$	3.25	0.6	2.5	% of solids
k_1	1.0	1.0	3.0	yr^{-1}
k_2	5.0×10^{-5}	1.0×10^{-3}	2.0×10^{-3}	yr^{-1}
F_{O_2} $(x = 0)$	5.25	9.19	13.8	mmol m^{-2} d^{-1}
$Mn(IV)_o$	0.05	0.5	0‡	%
$Fe(III)_o$	0.01	0.2	0‡	%
C:N	106:22	106:25¶	106:25	(mole:mole)
$k_{calcite}$	30	500	300	yr^{-1}
$k_{aragonite}$	3	50	5	yr^{-1}

where:
$G_1(0)$ = concentration of the highly reactive organic matter at the sediment-water interface ($x = 0$)
$G_2(0)$ = concentration of the weakly reactive organic matter at the sediment-water interface ($x = 0$)
k_1 = first-order decay constant for the highly reactive organic matter
k_2 = first-order decay constant for the weakly reactive organic matter
F_{O_2} ($x = 0$) = flux of O_2 at the sediment-water interface
$Mn(IV)_o$ = initial solid Mn(IV) concentration, i.e. $x = 0$
$Fe(III)_o$ = initial solid Fe(III) concentration, i.e. $x = 0$
C:N = Carbon to Nitrogen mole ratio in the decaying organic matter
$k_{calcite}$ = first-order dissolution constant for calcite
$k_{aragonite}$ = first-order dissolution constant for aragonite
‡Required with no dissolved metals measure in the porewaters.
¶Disagrees with simple stoichiometric modeling (see text). Probably not at steady state.

total solids that is composed of the more reactive organic type (as % carbon). The quantity of this reactive organic matter must be known to within about 0.1% in order to best simulate the O_2 profiles.

In these illustrated model results, the more reactive organic matter has a rate constant of 1–3 yr^{-1} and surface abundances of 0.1%, 1.7% and 2.5% at Stations 3, 4 and 5, respectively. Such material represents a yearly input of fresh organic matter, primarily from the Spring bloom that occurs at all these stations. Because of its high reactivity, this organic matter decays away rapidly in the first centimeter of the sediment and would be difficult to detect in our analyses of the solid phase (see Mucci *et al.,* 1999). The large difference between $G_1(0)$ at Station 3 and that at the other two stations may be disconcerting, particularly given the similar oxygen demands. An explanation lies with the large differences in mixing rates between stations (see the Parameter values section above and Mulsow *et al.,* 1998). The surficial OM concentrations are lower at Station 3 because mixing is so much more intense there. However, D_B was as large as 0.72 cm^2 yr^{-1} at Station 4 in the Winter of 1993 and 0.81 cm^2 yr^{-1} at Station 5 in the Summer of 1993. If such large values were used in the model, the calculated $G_1(0)$ values would be cut by more than half.

Mixing coefficient values are also greater if porosity gradients are included in the mixing model (see Table 4 of Mulsow *et al.,* 1998). This analysis highlights the need for accurate estimates of mixing rates for use in diagenetic models, particularly since reactive organic carbon is difficult to measure directly. In fact, this point is true of all solid-phase-based models, e.g. Aller (1994).

The more refractory organic matter has reactivities between $0.05–2 \times 10^{-3}$ yr^{-1}, and it is most abundant at Station 3 and least abundant at Station 4. These numbers are derived from the ΣCO_2 profiles, discussed further below. The abundance of more refractory carbon at Station 3 is consistent with the idea that the sandy shelf areas of the eastern Gulf of St. Lawrence eventually export most of their carbon and that this material is old and of low reactivity by the time it settles at this station.

b. Nitrate

The greatest discrepancies between the model and data occur with the nitrate profiles (Fig. 2). The Station 3 nitrate data are not plotted as the measurements are so low that they may suffur from analytical problems. The Station 4 nitrate data drop more rapidly in the first centimeter than expected from theory, while Station 5 data display a larger than expected maximum in the first centimeter.

The Station 4 data are much lower than observed in some other continental shelf sediments; e.g., Fernex *et al.* (1989), but not unlike the data reported at the S_4 Station by Canfield *et al.* (1993). CANDI incorporates traditional nitrification in the O_2 zone and predicts a rise to a maximum of 19 μM, followed by a rapid depletion to essentially zero nitrate by a depth of 1.5 cm, as observed in other coastal sediments; e.g., Enoksson and Samuelsson (1987) and Lohse *et al.* (1993). Luther *et al.* (1997) invoke a reaction between MnO_2 and ΣNH_3 in order to explain the apparent lack of nitrification of ammonia that is produced by sulfate reduction, i.e.

$$2NH_3 + 3MnO_2 + 6H^+ \rightarrow 3Mn^{2+} + N_2 + 6H_2O. \quad (8)$$

This reaction short-circuits the traditional Nitrogen cycle in sediments that takes ammonia to di-nitrogen via nitrate. This reaction was not included in the current version of CANDI, which may account for the discrepancy between the data and the model at Station 4.

Station 5 data, in contrast, exhibit the classic subsurface maximum due to sequential nitrification during O_2 reduction and subsequent denitrification; such distributions have previously been reported in continental rise sediments; e.g., Cai *et al.* (1995). The oddity is the magnitude of the NO_3^- rise; the increase is four times larger than can be explained by CANDI. An increase of this size is dwarfed only by that reported by Billen (1982) for sandy sediments in the Southern Bight of the North Sea. CANDI's results are completely consistent with the rise predicted by other models under similar circumstances; e.g., Jahnke *et al.* (1982), Wang and Van Cappellen (1996), and Soetaert *et al.* (1996), and actual maxima observed in other continental margin sediments; e.g., Christensen and Rowe (1984), Enoksson and Samuelsson (1987), Kemp *et al.* (1990), Devol and Christensen

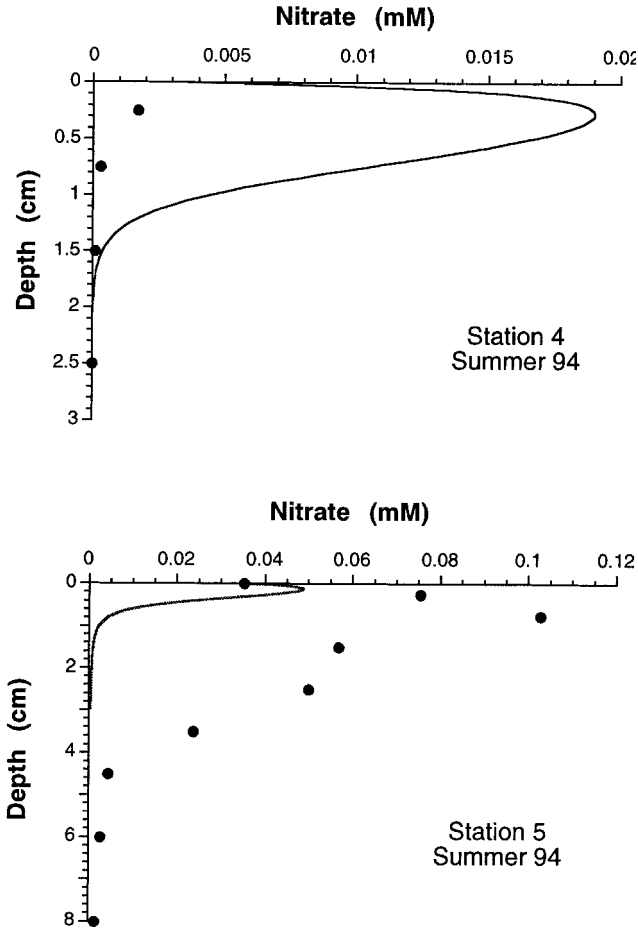

Figure 2. Nitrate data from Stations 4 and 5. Solid lines are predicts from CANDI, based on a C:N ratio of 106:25. Reasons for the mismatch are explored in the text.

(1993), and Lohse *et al.* (1993). Billen (1982) quantitatively accounts for his large maximum by oxidation of ammonia, produced deeper in the sediment by anaerobic respiration. Nitrification of upward diffusing ammonia is already part of CANDI; i.e., reaction (11) in Boudreau (1996a), but the diffusive flux of ammonia at Station 5 is simply not strong enough to generate the observed maximum. Another explanation must be sought.

One possibility for the anomalous nitrate peak at Station 5 rests in lowering the C/N ratio of the decaying organic matter in the aerobic zone. Currently, this ratio is set to the same value calculated for the anaerobic zone ammonia data; i.e., C/N = 4.24 (Table 2). However, this value is already remarkably small, as Canfield *et al.* (1993) cite 8.85 ± 3.7 as typical of continental margin sediments. A reduction to smaller than 0.2 would be

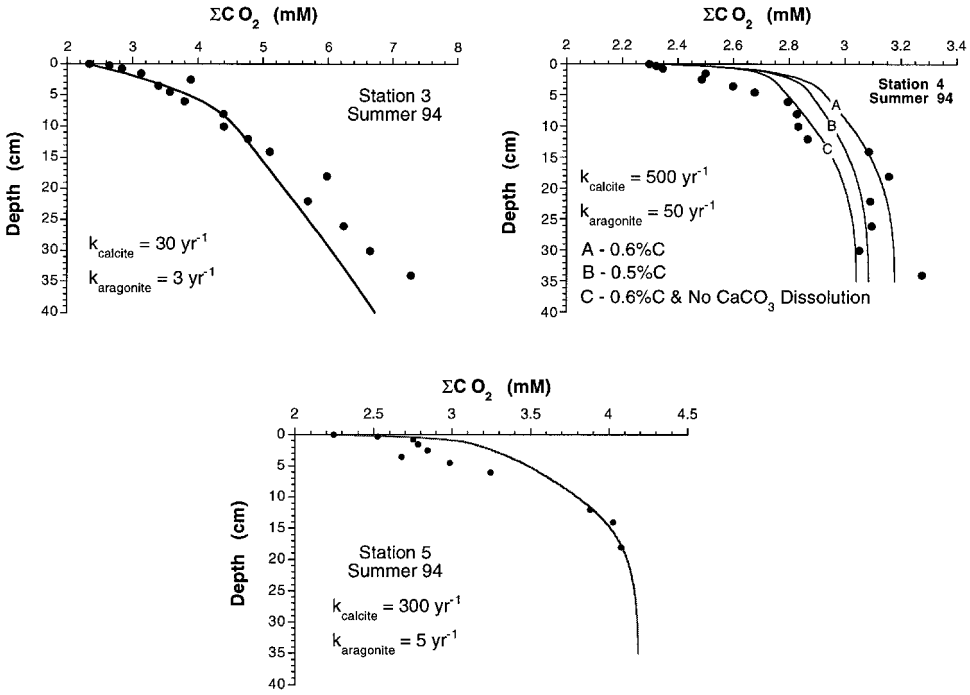

Figure 3. Plots of total inorganic carbon with depth at each of the three CJGOFS stations. The effect of aragonite and calcite dissolution is displayed in the Station 4 diagram. The % organic carbon refers to the less reactive type. The other diagrams contain the dissolution rate constants used to obtain the model lines.

necessary to explain the data, and that is highly unlikely. Another possibility is lysing bacterial cells that have stored nitrate (e.g., Fossing *et al.,* 1995) during squeezing; nevertheless, we observed no evidence of unusual bacterial mats, nor were the environmental conditions necessarily conducive to their growth. Irrigation could play a role in generating this peak; however, calculations of the effects of irrigation alone, presented in the ammonia section below, do not support this idea. Finally, the excess nitrate may be linked to unusual behavior of ammonia at this site (again see below).

c. Total CO_2

Our ΣCO_2 data are displayed in Figure 3. The initial increase (slope) in ΣCO_2 is dictated by oxic organic matter decay in the upper 2 cm at each site, while the final (asymptotic) amount of ΣCO_2 is largely controlled by the amount of sulfate reduction, with lesser contributions from $CaCO_3$ precipitation. Dissolution of calcite and aragonite also modestly alter CANDI's predictions of the ΣCO_2 data near the surface, and this is discussed further below. CANDI calculates that the porewaters are undersaturated with respect to calcite in the upper 1–3 cm, whereas they are supersaturated with respect to this mineral below these

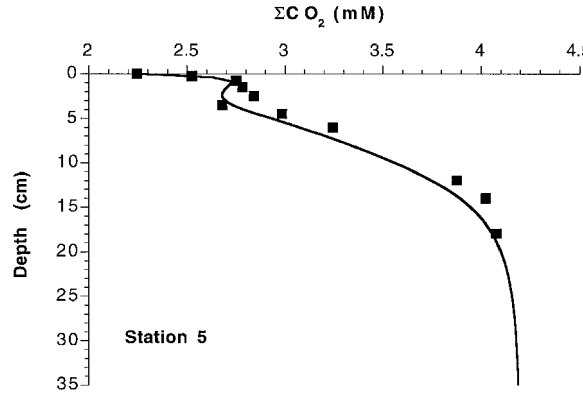

Figure 4. A model refit of the ΣCO_2 data for Station 5 that includes irrigation at a rate of 50 yr^{-1} and a spatial dependence given by Eq. (9) of the text; otherwise, the parameter values are the same as those in Figure 3.

depths. XRD analyses show that calcite is abundant in these sediments, but aragonite was not detected; however, pteropods are quite common in sediment trap material (Mucci *et al.,* 1999).

Station 3 sediments have the greatest amount of slowly reactive organic matter (3.25%, Table 2), and this fact is reflected in the much higher ΣCO_2 concentrations observed at depth. CANDI's slight under-prediction of ΣCO_2 below 30 cm may indicate the existence of another yet more slowly reactive organic matter fraction.

Station 5 has nearly as much of the second organic matter type, but CANDI indicates that it is substantially more reactive than at Station 3; thus, the decomposition occurs closer to the sediment-water interface and more of the ΣCO_2 produced escapes the sediments. The net result is that the asymptotic ΣCO_2 concentration is decidedly lower at Station 5. In addition, the dip in ΣCO_2 between 5 and 10 cm suggests a process that removes ΣCO_2; e.g., irrigation and/or $CaCO_3$ precipitation. The typical effects of irrigation are displayed in Figure 4, and they bring the model into close agreement with the data. These latter results were obtained by assuming that irrigation is a nonlocal exchange with a rate given by

$$R_{\text{irrigation}} = \frac{\eta}{2}\{1 - \tanh(x - x^*)\}[C_o - C] \tag{9}$$

where η is the irrigation rate constant, tanh() is the hyperbolic tangent function, x^* is a depth where irrigation begins to decline, C_o is the concentration of the solute in question in the overlying waters. The Figure 4 results were obtained with $\eta = 50$ yr^{-1} and x^* of 4 cm Larger values of either parameter lead to less optimal fits and the appearance of O_2 at depth in the sediment.

The ΣCO_2 profile at Station 4 is somewhat over-predicted at shallow depths; i.e., too much production. This discrepancy may be related to nonsteady state effects, as discussed below in the section on the Mn^{2+} results.

In these model predictions, we have added enough dissolution of both calcite and aragonite, as first-order processes in their own saturation states (Hales and Emerson, 1997); i.e.,

$$R_{\text{aragonite}} = k_{\text{aragonite}} \left[K_{\text{aragonite}} - (Ca^{2+})(CO_3^{=})\right] \tag{10}$$

and

$$R_{\text{calcite}} = k_{\text{calcite}} \left[K_{\text{calcite}} - (Ca^{2+})(CO_3^{=})\right] \tag{11}$$

to eliminate their respective undersaturations. In these equations, $k_{\text{aragonite}}$ and k_{calcite} are the rate constants, whereas $K_{\text{aragonite}}$ and K_{calcite} are the solubility products, respectively. Dissolved carbonate concentrations were calculated dynamically from the observed pH (Mucci *et al.,* 1999) and the model ΣCO_2. Comparison of the calculated rate constants with previously modelled values is difficult because recent studies have assumed nonlinear kinetics; however, the order of magnitude consistency between stations is encouraging and may indicate useful values. The difference between CANDI fits with and without dissolution is illustrated with the Station 4 results of Figure 3. The ΣCO_2 modifications engendered by these mineral dissolutions are modest, but probably observable.

d. Ammonia

Figure 5 contains the total ammonia data for our three stations, as well as the fits from CANDI. The free parameter available for these fits is the C/N ratio of the decaying organic matter. Sensitivity to this parameter is illustrated in the Station 4 diagram of Figure 5. The model output is reasonably sensitive to the C/N ratio, and the values required in order to fit the data at all stations are in the narrow range of 106:22 to 106:25, i.e. 4.82 to 4.24. This compares with a mean C/N of 15 from solid phase analyses at both Stations 3 and 4 (CJGOFS unpublished data, K. Juniper, Pers. Commun.). These results would suggest strong preferential regeneration of N at all three sites.

As with the ΣCO_2, the prediction of the ammonia profile at Station 3 is generally well represented, with a slight underestimation of the asymptotic concentration at depth. Again, this is probably attributable to another, slower reacting organic matter component. The Station 4 data seem well simulated. The Station 5 ammonia data are perceptively lower in the top 20–25 cm than predicted by the model. The similarity to the anomaly in the ΣCO_2 data suggests that irrigation might be responsible.

In order to determine the internal consistency of these results, the data and model results are also displayed on "stoichiometric" type plots in Figure 6, and these diagrams reveal some important facts not apparent in the property-depth plots. In particular, the modeled regeneration ratio (106:22) at Station 3 is very close to that derived using a simple Berner-type model (i.e., 106:21.2), which is a statistical best fit. Strong preferential regeneration of Nitrogen does, indeed, occur at this station. More and more, Station 3 emerges as consistent with the predictions of standard steady-state diagenetic theory.

The plot for Station 4 in Figure 6 displays a striking discrepancy between the data and

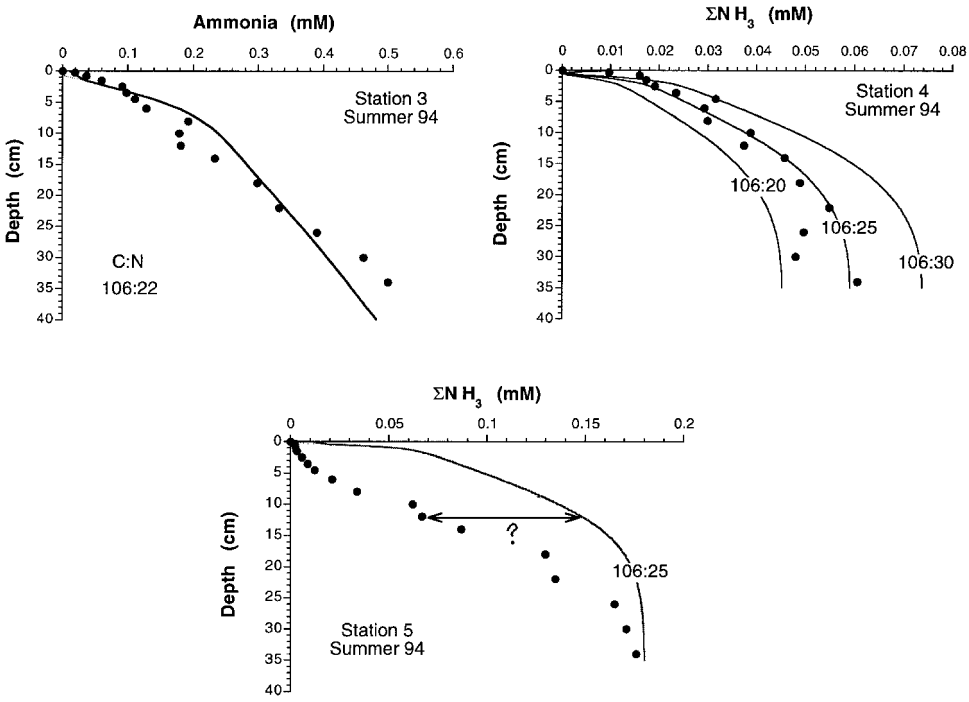

Figure 5. Total ammonia profiles for the three stations and the CANDI model fits. The C:N ratio was the free parameter available in fitting these data; its value is indicated in each diagram. The question mark in the Station 5 plot indicates a sink for ammonia, not originally included in the model.

the CANDI-generated results. The data plot on a simple linear trend, equivalent to a C:N regeneration ratio of 106:10.6; meanwhile, the CANDI-based prediction is a curved line that only roughly approximates the data and suggests preferential regeneration. The CANDI line in Figure 6 is curved because two strong sources of C and N to the porewaters are needed to explain the combined O_2, ΣCO_2 and ΣNH_3 data if steady state is operative. The data make no such suggestion and the underlying assumption to the model, i.e. steady state, must come into question. This latter point finds strong support from the Mn^{2+} data, as discussed further below.

Finally, the initial Station 5 plot in Figure 6 without irrigation clearly shows that the model result fails to reproduce the data. These data form a regular curved trend on this plot, while the model line, after an initial curved segment, is a straight line as in a conventional stoichiometric plot. The difference between model and data is the opposite of that seen at Station 4. Curvature of this variety in the data arises from any process that creates an additional source or sink of these solutes, beyond that from the decay of a single organic matter type. Irrigation would constitute such a sink; consequently, the ΣNH_3 data were refit using the amount of irrigation implied by the fit to the ΣCO_2 in Figure 4; i.e., $\eta = 50\ yr^{-1}$

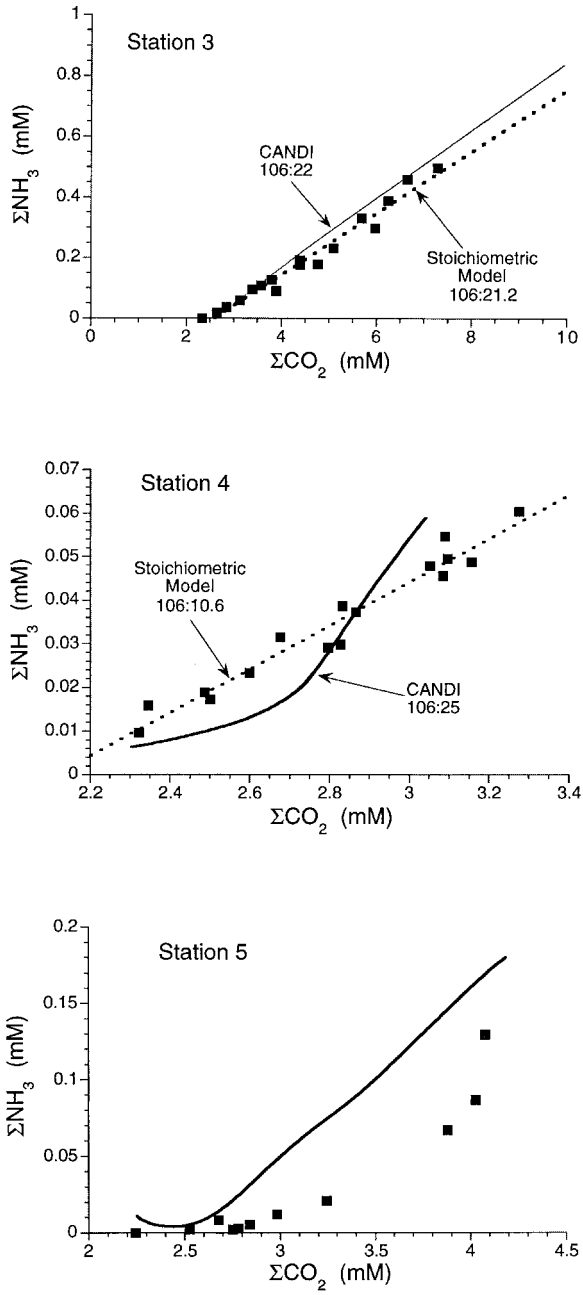

Figure 6. ΣCO_2-ΣNH_3 stoichiometric plots for the data and model results. The solid line represents the output from CANDI. The dashed line, where present, is a simple linear regression on the data, used in a Berner-type stoichiometric model.

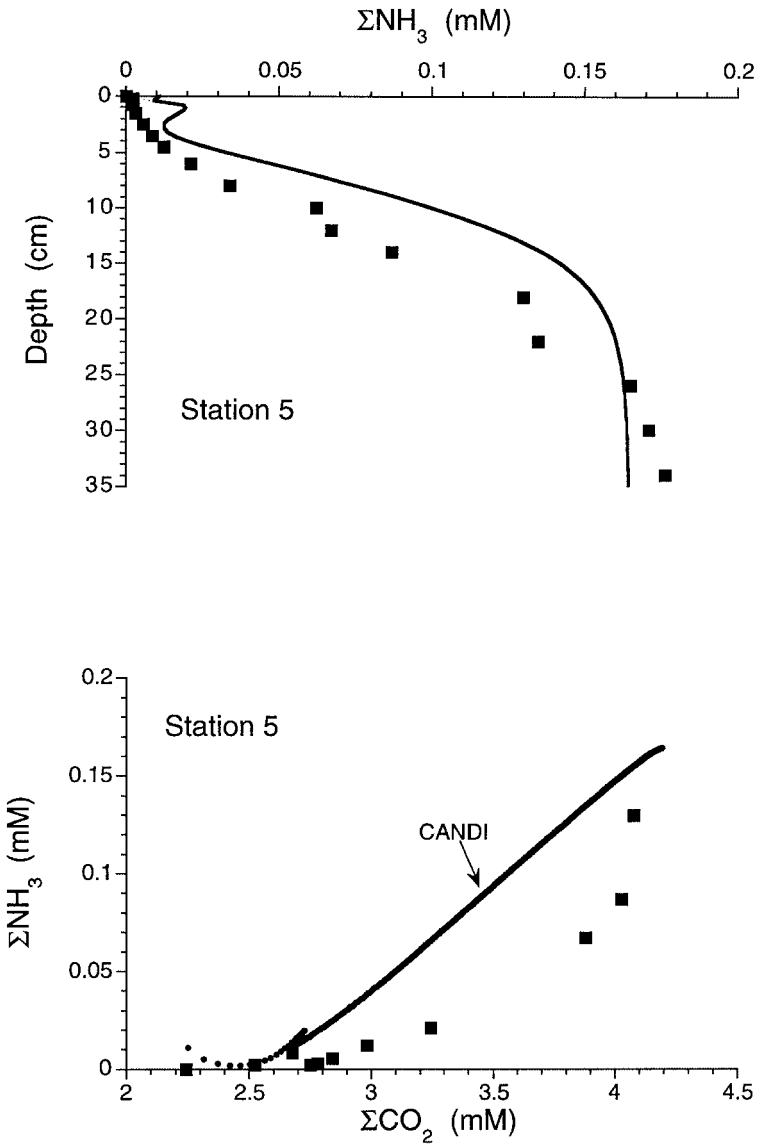

Figure 7. Top diagram is a plot of the Station 5 total ammonia data along with the CANDI output (solid line) that includes the same degree of irrigation as in Figure 4. The bottom diagram is a ΣCO_2-ΣNH_3 stoichiometric plot for this same station that includes the CANDI results (dots merging to a solid line).

and x^* of 4 cm in Eq (9). The result is illustrated in the top plot of Figure 7. While an improvement, a closer fit to the data above 20 cm, cannot be obtained without sacrificing the agreement below this depth, and vice-versa. Arguments about the goodness of this fit are, however, largely moot, as the resulting stoichiometric plot exhibits no improvement,

and the amount of irrigation needed to "fix" this disparity would create unacceptable problems in the other profiles.

The CANDI results in Figure 7 tell us that a process other than irrigation, as we currently understand it, must be responsible for the curvature in the Station 5 stoichiometric plot. The sense of the curvature argues that ΣNH_3 is removed preferentially to ΣCO_2. Deep oxidation of the ammonia to nitrate is, nevertheless, unlikely because no NO_3^- is found in the porewaters at the required depths, and neither O_2 nor MnO_2 appears to be available as an oxidant in the appropriate depth range. Additionally, crystalline ferric minerals are unlikely candidates as oxidants because of the paucity of dissolved iron in the porewaters at this site (Luther *et al.,* 1998). Station 5 is also marked by anomalous "excess" nitrate in the near surface porewater (Fig. 2). We are tempted to speculate that the "missing" ammonia is transported to the upper 3 cm, rather than the overlying seawater, where it is oxidized with O_2. This transport would be selective to ammonia, as the effects do not appear in the ΣCO_2 profile, which suggests solute-specific transport. A possibility is irreversible NH_3-NH_4^+ adsorption onto solids and bioturbation into the O_2 zone for oxidation. The irreversibility of such a process would be necessary because linear reversible adsorption would not create curvature in a stoichiometric plot, as shown by Berner (1977, 1980). Another, perhaps vague, mechanisms would be a selective biologically mediated transport. We possess no further evidence in regard to this phenomena and must abandon further comment unless future studies provide more information.

e. Manganese

The dissolved Mn^{2+} concentrations are plotted in Figure 8 for Stations 3 and 4. Our voltammetric microelectrode did not detect any dissolved manganese in the upper 10 cm at Station 5 (5 μM detection limit), which is consistent with the lack of reactive solid Mn at this station reported by Luther *et al.* (1998). The manganese data at the remaining two stations have a number of noteworthy features.

At neither station does Mn^{2+} overlap the O_2 profiles, and Aller (1990) and Luther *et al.* (1997) have advanced that Mn^{2+} is oxidized by NO_3^- (or iodate) before the former reaches the oxic zone; i.e., via reaction (2) given above. We have tested this hypothesis with CANDI. The Station 4 diagram in Figure 8 illustrates the CANDI-predicted Mn^{2+} profiles with and without reaction (2). Whereas addition of reaction (2) certainly shifts the predicted profile downward, away from the oxic zone, the predicted Mn^{2+} profile is still some 2 cm above the data. Reaction (2) alone cannot account for the discrepancy. A nonsteady state history may be at work at Station 4 — for a related example, see Gobeil *et al.* (1997). Oxygen might not be penetrating as deeply as in the recent past. Such a situation could occur as a result of a number of factors, including rapid increase in the delivery of highly reactive organic matter or a sudden decrease in the rate of mixing, as perhaps suggested by the D_B values calculated by Mulsow *et al.* (1998). Changes in bottom water O_2 content might have the observed effect, but then the Mn^{2+} profile should have time to adjust to that type of change.

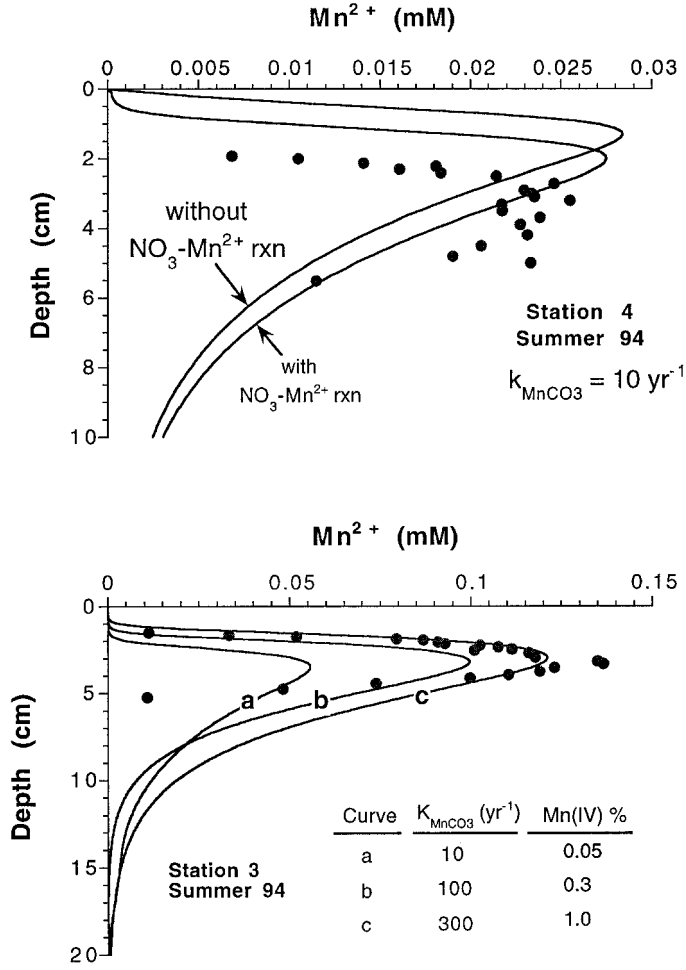

Figure 8. Dissolved manganese distributions at Stations 3 and 4. The model curves in the top diagram (Station 4) illustrate the effect of reaction (2); i.e., Mn^{2+} oxidation by NO_3^-. The bottom diagram shows the effect of varying the Mn^{2+} removal rate constant and initial Mn(IV) at Station 3.

The Mn^{2+} profiles and CANDI's predictions are in much better agreement at Station 3. This calculation is inclusive of reaction (2), and it was driven with a surficial MnO_2 content of 1% of solids by dry weight, which is similar to the data reported by Luther *et al.* (1998). The solid phase Mn data and that predicted by the model are not presented here, but differ in their rates of decrease with depth; however, the solids data comes from a separate core, and we fear strong lateral heterogeneities in the solid phase data; e.g., Smith and Schafer (1984). The main discrepancy between model and data now centers on the backside of the Mn^{2+} peak. Figure 8 displays theoretical curves for three different removal rate constants

and initial solid-Mn(IV) concentrations at the sediment-water interface; the curve labelled c begins to supply a reasonable simulation of the position of the front and the magnitude of the peak, but not the precipitous decline. In fact, we have found no combination of $k_{\text{Mn-loss}}$ value and Mn(IV) input that could match the data.

The problem seems to revolve around the kinetics assumed in Eq. (6). The reaction rate is linear in the Mn^{2+} concentration. This means that Mn^{2+} below the maximum will decrease to undetectable levels with depth in an exponential-like manner; i.e., attaining zero concentration only at infinity. This type of decline is not rapid enough. The rapid decline in the data indicate undetectable Mn^{2+} at a finite depth of about 6 cm. A higher-order power in the Mn^{2+} concentration will lead to an even gentler decline, approximately proportional to x^{-n}, where n is the order of reaction. To obtain a rapid decline to essentially zero values at a finite depth, the order must be less than 1 (Boudreau, 1997). Consequently, Figure 8 appears to constitute evidence that the overall kinetics of Mn^{2+} removal are fractional order in that species' concentration. Such kinetics have been argued to result from multiple, competing reactions (e.g., Shoemaker *et al.,* 1981). We cannot, however, explore this suggestion further, as CANDI and all other diagenesis codes in current use cannot deal properly, in a numerical sense, with such kinetics.

f. Reactive carbon balance

Among CANDI's various outputs are estimates of the fraction of the total organic matter input at these stations that is consumed by the various possible oxidants at steady state; i.e., O_2, NO_3^-, Mn(IV), Fe(III), $SO_4^=$ and self-oxidation (methanogenesis). Clearly the Station 4 predictions must be regarded with some suspicion, as nonsteady-state effects are not included.

The information presented in Table 3 is valuable in at least two respects. Firstly, it constitutes a check on carbon balance in the model, which in our cases is balanced to no worse than 0.1%. Secondly, such numbers allow comparison with diagenesis at other sampled sediments, independent of the absolute magnitude of the carbon input. A selection of similar data from other coastal and marginal sediments is also included in Table 3. A caveat must be kept in mind when considering the results in Table 3. Our CANDI results do not produce as much FeS and FeS_2 as recorded in the sediments (Mucci *et al.,* 1999), because, in reality, a second slowly reacting source of iron allows FeS and FeS_2 to be formed progressively with depth into the sediment (Canfield, 1989). CANDI does not presently have the capability to deal with a second iron source. Consequently, more of the H_2S produced by sulfate reduction is precipitated deep in the sediment and buried, rather than transported upward and oxidized with O_2 or precipitated as FeS-FeS_2 in the upper decimeters of the sediment; therefore, the role of O_2 as an OM oxidant is minimized and that of sulfate reduction is conversely maximized. Nevertheless, the Table 3 results remain highly informative.

The results in Table 3 emphasize that Station 3 is, by far, the more reducing, and that the shallowest site, Station 4, is most oxic. In fact, Station 3 is remarkably similar to the 190 m

Table 3. Percent of carbon oxidized by various oxidants at the CJGOFS sites assuming steady state and some other coastal and marginal sites available in the literature‡.

Site†	O_2	NO_3^-	Mn(IV)	Fe	$SO_4^=$	CH_4§	Total¶
3	15.0	3.65	15.9	1.63	52.7	0.97	100.0
4	73.7	14.2	2.39	0.65	8.84	0.15	100.1
5	53.4	20.3	0.0	0.0	25.9	0.46	100.1
S_4	13.6	3.2	0.0	32.1	51.1	—	100
S_6	17.4	3.8	0.0	50.9	27.9	—	100
S_9	3.6	5.7	90.7	0.0	<1.0	—	100
FP1	6.0	13.5	—	—	80.5*	—	100
FP2	9.4	23.5	—	—	67.1*	—	100
FP3	9.7	11.7	—	—	78.6*	—	100
FP4	13.6	14.8	—	—	71.6*	—	100
LIS1	8.1	18.8	—	—	73.1*	—	100
LIS2	3.3	14.1	—	—	82.6*	—	100
QP2	68.6−	6.8−	1.3−	0.03−	6.0−	—	100
	74.1	12.1	2.3	0.06	10.8	—	100

‡Rates of OM oxidation by O_2 are somewhat minimized and those of sulfate reduction are maximized by our underestimation of FeS-FeS_2 burial.

†S_4, S_6 and S_9 are the Skaggerak sites (Canfield *et al.,* 1993). FP1, FP2, FP3 and FP4 are from Flax Pond, New York, as sampled on 6/13/87, 7/29/87, 9/22/87 and 12/11/87, respectively (Mackin and Swider, 1989). LIS1 and LIS2 are values from Mackin and Swider (1989) Long Island Sound Station 9, sampled on 1/28/87 and 8/6/87, respectively. QP2 is a continental rise site at 3160, east of Cap Hatteras, reported by Heggie *et al.* (1987).

§Self-oxidation to produce methane.

*Mackin and Swider assume that carbon oxidation other than with O_2 and NO_3^- is mainly attributable to $SO_4^=$.

¶Totals for CANDI can be different than 100% because of errors in numerical approximations.

S_4 site studied by Canfield *et al.* (1993) in the Skaggerak; specifically, oxygen utilization accounts for only ~15% of carbon oxidation, while sulfate reduction amounts for ~52% of the total, at each site. The only significant difference was the metal oxide contributions. At S_4, Mn(IV) and Fe(III) account for ~0.0 and 32.1% of the total reduction, whereas these numbers are ~16 and 1.6%, respectively, at Station 3. The Station 4 metal contributions could easily be in error because of numerous assumptions made in order to run the model (e.g., the iron input); likewise, Canfield *et al.* (1993) state that because of errors and assumptions, the Mn(IV) contribution could be as high as 10%. Therefore, the similarity may be more striking than suggested in Table 3. At both sites, most of the oxygen is used to oxidize reduced by-products (i.e., Fe^{2+}, Mn^{2+}, H_2S and NH_3), rather than organic matter. Metal oxide reduction definitely rivals O_2 utilization in the carbon balance. Estimates for Flax Pond, New York, and Long Island Sound bear some similarity to Station 3, in that $SO_4^=$ is a dominant oxidant and O_2 is not; however, further comparison is not possible because metal oxide contributions were not resolved by Mackin and Swider (1989).

In contrast to Station 3, our Station 4 strongly resembles the deep continental rise QP2

site from Heggie *et al.* (1987). Oxygen consumption dominates the carbon balance (~74%), followed by nitrate and sulfate, then quite minor contributions from the metal oxides. The QP2 and Station 4 balances are not that different from the estimates for the deep-sea MANOP sites M, H and C (Bender and Heggie, 1984). What is notable is that Station 4 is a mud in only 230 m of water, while the deep sea sites are all below 3000 m; could this be the result of our steady state assumption? Station 5, at an intermediate depth, is more reduced than Station 4, but inclusion of irrigation, as in Figure 4, does not appreciably alter the results given in Table 3.

6. Conclusions

The object of diagenetic modeling is to advance our understanding of diagenesis through quantitative and rigorous analysis, particularly of data. If models and observations were always in accord, then we might conclude that we possessed perfect theoretical comprehension of diagenesis, a highly improbable situation indeed. (This state would be akin to that of late 19th-Century physicists who mistakenly believed that their discipline was essentially complete.) Therefore, all diagenetic data sets should be subject to quantitative modeling (in its broadest interpretation) in order to aid in the discovery of new or unappreciated phenomena or to indicate how the theory itself needs improvement.

In this spirit we have applied the diagenesis code CANDI (Boudreau, 1996a) to integrate our understanding of the porewater data at three sites on the Canadian continental margin. From this analysis we have been able to establish that the sediment at Station 3 in the Cabot Strait is well described by the standard, steady-state, diffusion-reaction theory within CANDI. On the other hand, our modeling indicates that the porewaters at Stations 4 and 5, on the Scotian Shelf and Slope, respectively, follow less orthodox behavior. Specifically, Station 4 appears to be in a nonsteady state, while Station 5 is not only irrigated (see Fig. 4), but seemingly subject to unusual transport and oxidation of ammonia. More work needs to be done to expand on this latter possibility.

Furthermore, our modeling has allowed us to reach a number of secondary conclusions, including:

(1) At least two types of reactive OM exist at each station: one that decays on a yearly basis and one that decomposes on decadal or longer time scales. The calculated initial amounts of these organic matter types is a sensitive function of the mixing rates; consequently, accurate assessment of mixing must become a priority in studies of early diagenesis.

(2) Ammonia is preferentially regenerated at Station 3 at an unusually high ratio of 22 N to 106 C. Simple Berner-type stoichiometric modeling verifies this finding.

(3) The dissolved manganese is affected by oxidation with nitrate (and possibly iodate). This process tends to separate the overlap between O_2 and Mn^{2+}; however, this is

not enough to explain the separation at Station 4, and nonsteady state effects are likely there.

(4) The decline in Mn^{2+} with depth is attributed to either co-precipitation as a carbonate or adsorption onto carbonates or FeS. The model fits suggest that the net kinetics of this process are fractional-order with respect to the Mn^{2+} concentration. Such net kinetics have been argued to result from multiple, simultaneous and competing reactions (e.g., Shoemaker *et al.,* 1981).

(5) Assuming steady-state, the balance of carbon oxidants shows that organic matter oxidation is dominated by O_2-reduction at Station 4, at only 230 m depth, whereas Station 3, at 530 m, is dominated by suboxic-anoxic diagenesis, much like an organic-rich coastal sediment.

Acknowledgments. B. Boudreau, A. Mucci and B. Sundby were supported by an NSERC CSP grant, awarded for the Canadian JGOFS Project (Benthic Processes Study). G. Luther received support from a NOAA grant (NA16RG0162-03). We would like to express our sincere appreciation to the postdoctoral fellows who participated in gathering the data that we modeled in this paper: Pierre Anschutz, Takashi Arakaki, Brent Lewis, Sandor Mulsow, and Shaojun Zhong. We greatly appreciate the reviews provided by R. C. Aller and an anonymous individual.

REFERENCES

Aller, R. C. 1990. Bioturbation and manganese cycling in hemipelagic sediments. Phil. Trans. Royal Soc. London, *A331,* 51–68.

—— 1994. The sedimentary Mn cycle in Long Island Sound: Its role as intermediate oxidant and the influence of bioturbation, O_2, and C_{org} flux on diagenetic reaction balance. J. Mar. Res., *52,* 259–295.

Aller, R. C. and P. D. Rude. 1988. Complete oxidation of solid phase sulfides by manganese and bacteria in anoxic marine sediments. Geochim. Cosmochim. Acta, *52,* 751–765.

Anschutz, P., S. Zhong, B. Sundby, A. Mucci and C. Gobeil. 1998. Burial efficiency of phosphorus and the geochemistry of iron in continental margin sediments. Limnol. Oceanogr., *43,* 53–64.

Arakaki, T. and J. W. Morse. 1993. Coprecipitation and adsorption of Mn(II) with mackinawite (FeS) under conditions similar to those found in anoxic sediments. Geochim. Cosmochim. Acta, *57,* 9–14.

Bender, M. L. and D. T. Heggie. 1984. Fate of organic carbon reaching the deep-sea floor: a progress report. Geochim. Cosmochim. Acta, *48,* 1987–2004.

Berner, R. A. 1977. Stoichiometric models for nutrient regeneration in anoxic sediments. Limnol. Oceanogr., *22,* 781–786.

—— 1980. Early Diagenesis: A Theoretical Approach, Princeton University Press, Princeton, NJ, 241 pp.

—— 1982. Burial of organic carbon and pyrite in the modern ocean: its geochemical and environmental significance. Am. J. Sci., *282,* 451–473.

Billen, G. 1982. An idealized model of nitrogen recycling in marine sediments. Am. J. Sci., *282,* 512–541.

Boudart, M. and G. Djéga-Mariadassou. 1984. Kinetics of Heterogeneous Catalytic Reactions, Princeton University Press, Princeton, NJ, 222 pp.

Boudreau, B. P. 1996a. A method-of-lines code for carbon and nutrient diagenesis in aquatic sediments. Comput. Geosci., *22,* 479–496.

—— 1996b. The diffusive tortuosity of fine-grained unlithified sediments. Geochim. Cosmochim. Acta, *60,* 3139–3142.

—— 1997. Diagenetic Models and their Implementation, Springer Verlag, Heidelberg, 414 pp.

Boudreau, B. P. and J. T. Westrich. 1984. The dependence of bacterial sulfate reduction on sulfate concentration in marine sediments. Geochim. Cosmochim. Acta, *48,* 2503–2516.

Bouldin, D. R. 1968. Models for describing the diffusion of oxygen and other mobile constituents across the mud-water interface. Jour. Ecol., *56,* 77–87.

Boyle, E. A. 1983. Manganese carbonate overgrowths on Foraminifera tests. Geochim. Cosmochim. Acta, *47,* 1815–1819.

Buckley, D. E. 1991. Deposition and diagenetic alteration of sediment in Emerald Basin, the Scotian Shelf. Cont. Shelf Res., *11,* 1099–1122.

Cai, W.-J., C. E. Reimers and T. Shaw. 1995. Microelectrode studies of organic carbon degradation and calcite dissolution at a California continental rise site. Geochim. Cosmochim. Acta, *59,* 497–511.

Canfield, D. E. 1989. Reactive iron in marine sediments. Geochim. Cosmochim. Acta, *53,* 619–632.

—— 1993. Organic matter oxidation in marine sediments, *in* Interactions of C, N, P and S Biogeochemical Cycles, R. Wollast, L. Chou and F. Mackenzie, eds., NATO-ARW, Springer Verlag, Berlin, 333–363.

Canfield, D. E., B. B. Jørgensen, H. Fossing, R. Glud, J. Gundersen, N. B. Ramsing, B. Thamdrup, J. W. Hassen, L. P. Neilsen and P. O. J. Hall. 1993. Pathways of carbon oxidation in three continental margin sediments. Mar. Geol., *113,* 27–40.

Christensen, E. R. 1982. A model for radionuclides in sediments influenced by mixing and compaction. J. Geophys. Res., *87,* 566–572.

Christensen, J. P. and G. T. Rowe. 1984. Nitrification and oxygen consumption in northwest Atlantic deep-sea sediments. J. Mar. Res., *42,* 1099–1116.

Devol, A. H. and J. P. Christensen. 1993. Benthic fluxes and nitrogen cycling in sediments of the continental margin of the eastern North Pacific. J. Mar. Res., *51,* 345–373.

Enoksson, V. and M.-O. Samuelsson. 1987. Nitrification and dissimilatory ammonium production and their effects on nitrogen flux over the sediment-water interface in bioturbated coastal sediments. Mar. Ecol. Prog. Ser., *36,* 181–189.

Fernex, F., R. Baratie, D. Span and L. V. Fernandes. 1989. Variations of nitrogen nutrient concentrations in the sediment pore waters of the northwestern Mediterranean continental shelf. Cont. Shelf Res., *9,* 767–794.

Fossing, H., V. A. Gallardo, B. B. Jørgensen, M. Hüttel, L. P. Nielsen, H. Sultz, D. E. Canfield, S. Forster, R. N. Glud, J. K. Gundersen, J. Küver, N. B. Ramsing, A. Teske, B. Thamdrup and O. Ulloa. 1995. Concentration and transport of nitrate by the mat-forming sulfur bacterium Thioploca. Nature, *374,* 713–715.

Gobeil, C., R. W. Macdonald and B. Sundby. 1977. Diagenetic separation of cadmium and manganese in suboxic continental margin sediments. Geochim. Cosmochim. Acta, *61,* 4647–4654.

Grant, J., C. W. Emerson, B. T. Hargrave and J. L. Shortle. 1991. Benthic oxygen consumption on the continental shelves off Eastern Canada. Cont. Shelf Res., *11,* 1083–1097.

Grehan, A. J., P. Scaps, G. Desroisiers, K. Juniper and G. Stora. 1994. Vertical macrofaunal distribution in the soft sediments of the Gulf of St. Lawrence and the Scotian continental margin. Vie Milieu, *44,* 101–107.

Hales, B. and S. Emerson. 1997. Evidence in support of first-order dissolution kinetics of calcite in seawater. Earth Planet. Sci. Lett., *148,* 317–327.

Heggie, D., C. Maris, A. Hudson, J. Dymond, R. Beach and J. Cullen. 1987. Organic carbon oxidation and preservation in NW Atlantic continental margin sediments, *in* Geology and Geochemistry of Abyssal Plains, P. P. E. Weaver and J. Thomson, eds., Geol. Soc. Special Publ. #31, 215–236.

Jahnke, R. A., S. R. Emerson and J. W. Murray. 1982. A model of oxygen reduction, denitrification, and organic matter mineralization in marine sediments. Limnol. Oceanogr., *27,* 610–623.

Kemp, W. M., P. Sampou, J. Caffrey, M. Mayer, K. Henriksem and W. R. Boynton. 1990. Ammonium recycling versus denitrification in Chesapeake Bay sediments. Limnol. Oceanogr., *35,* 1545–1563.

Kukulka, D. J., B. Gebhart and J. C. Mollendorf. 1987. Thermodynamic and transport properties of pure and saline water. Adv. Heat Transfer, *18,* 325–363.

Li, Y.-H. and S. Gregory. 1974. Diffusion of ions in seawater and in deep-sea sediments. Geochim. Cosmochim. Acta, *38,* 703–714.

Lohse, L., J. F. P. Malschaert, C. P. Slomp, W. Helder and W. van Raaphorst. 1993. Nitrogen cycling in North Sea sediments: interaction of denitrification and nitrification in offshore and coastal areas. Mar. Ecol. Progr. Ser., *101,* 283–296.

Luther, III, G. W., B. Sundby, B. L. Lewis, P. J. Brendel and N. Silverberg. 1997. Interactions of manganese with the nitrogen cycle: alternative pathways to dinitrogen. Geochim. Cosmochim. Acta, *61,* 4043–4052.

Luther, III G. W., P. J. Brendel, B. L. Lewis, B. Sundby, L. Lefrancois, N. Silverberg and D. B. Nuzzio. 1998. Simultaneous measurement of O_2, Mn, Fe, I^-, and S(-II) in marine pore waters with a solid state voltammetric microelectrode. Limnol. Oceanogr., *43,* 325–333.

Mackin, J. E. and K. T. Swider. 1989. Organic matter decomposition pathways and oxygen consumption in coastal marine sediments. J. Mar. Res., *47,* 681–716.

Middelburg, J. J., G. J. de Lange and C. H. van der Weijden. 1987. Manganese solubility control in marine porewaters. Geochim. Cosmochim. Acta, *51,* 759–763.

Mucci, A. 1988. Manganese uptake during calcite precipitation from seawater: conditions leading to the formation of a pseudokutnahorite. Geochim. Cosmochim. Acta, *52,* 1859–1868.

Mucci, A., B. Sundby, M. Gehlen, T. Arakaki and N. Silverberg. 1999. The fate of carbon in continental shelf sediments of Eastern Canada: a case study. Deep-Sea Res., (in press).

Mulsow, S., B. P. Boudreau and J. N. Smith. 1998. Bioturbation and porosity gradients. Limnol. Oceanogr., *43,* 1–9.

Pedersen, T. F. and N. B. Price. 1982. The geochemistry of manganese carbonate in Panama Basin sediments. Geochim. Cosmochim. Acta, *46,* 59–68.

Shoemaker, D. P., C. W. Garland, J. I. Steinfeld and J. W. Nibler. 1981. Experimental Physical Chemistry, 4th ed., McGraw-Hill, New York, 253 pp.

Silverberg, N., H. V. Nguyen, G. Delibrias, M. Koide, B. Sundby, Y. Yokoyama and R. Chesselet. 1986. Radionuclide profiles, sedimentation rates, and bioturbation in modern sediments of the Laurentian Trough, Gulf of St. Lawrence. Oceanol. Acta, *9,* 285–290.

Silverberg, N., B. Sundby, A. Mucci, S. Zhong, T. Arakaki, P. Hall, A. Tengberg and A. Hillemyr. 1999. Organic carbon mineralization and carnonate dissolution in sediments at the JGOFS sites in eastern Canada. Deep-Sea Res., (submitted).

Smith, J. N. and C. T. Schafer. 1984. Bioturbation processes in continental slope and rise sediments delineated by Pb-210, microfossil and textural indicators. J. Mar. Res., *42,* 1117–1145.

Soetaert, K., P. M. J. Herman and J. J. Middelburg. 1996. A model of early diagenetic processes from shelf to abyssal depths. Geochim. Cosmochim. Acta, *60,* 1019–1040.

Thomson, J., N. C. Higgs, I. Jarvis, D. J. Hydes, S. Colley, and T. R. S. Wilson. 1986. The behaviour of manganese in Atlantic carbonate sediments. Geochim. Cosmochim. Acta, *50,* 1807–1818.

Van Cappellen, P. and J.-F. Gaillard. 1996. Biogeochemical dynamics in aquatic sediments, *in* Reactive Transport in Porous Media, P. C. Lichtner, C. I. Steefel and E. H. Oelkers, eds., Reviews in Mineralogy, *34,* Mineralogical Society of America, Washington, DC, 335–376.

Van Cappellen, P., J.-F. Gaillard and C. Rabouille. 1993. Biogeochemical transformations in sediments: kinetic models of early diagenesis, *in* Interactions of C, N, P and S Biogeochemical Cycles, R. Wollast, L. Chou and F. Mackenzie, eds., NATO-ARW, Springer Verlag, Berlin, 401–445.

Van Cappellen, P. and Y. Wang. 1995. Metal cycling in surface sediments: modelling the interplay of transport and reaction, *in* Metal Contaminated Sediments, H. E. Allen, ed., Ann Arbor Press, 21–64.

Wang, Y. and P. Van Cappellen. 1996. A multicomponent reactive transport model of early diagenesis: application to redix cycling in coastal marine sediments. Geochim. Cosmochim. Acta, *60,* 2993–3014.

Received: *29 December, 1997;* revised: *21 July, 1998.*